AIAA AVIATION Forum
5-9 June 2017, Denver, Colorado
23rd AIAA/CEAS Aeroacoustics Conference

On the noise generated by the potential-core closing of temporally-developing subsonic jets

Christophe Bogey*
Laboratoire de Mécanique des Fluides et d'Acoustique
UMR CNRS 5509, Ecole Centrale de Lyon
69134 Ecully, France

Two temporally-developing isothermal round jets at a Mach number of 0.9 and diameter-based Reynolds numbers of 3,125 and 12,500 have been computed in order to investigate the sound waves produced by the closing of the jet potential core. The simulations are carried out using high-order finite differences on a grid of 940 million points extending up to 120 jet radii in the axial direction. For each case, ten runs are performed using different initial random perturbations in the jet shear layers, and their results are ensemble averaged. Snapshots and statistical properties of the jet flow and acoustic fields are first presented. Flow-noise correlations and conditional averages of the jet near field are then shown. The jet at a Reynolds number of 12,500 develops more rapidly, exhibits more fine turbulent scales, and generates more high-frequency acoustic waves than the jet at a Reynolds number of 3,125, as expected. In both cases, however, the flow fluctuations on the jet axis are strongly intermittent at the time of potential-core closing, and low-frequency acoustic waves are subsequently radiated in the downstream direction. Furthermore, the centerline flow fluctuations and these waves are found to be strongly correlated, as observed for spatially-developing jets. These results led us to calculate conditional averages of the jet near fields using a sampling synchronization with the minimum values of centerline axial velocity at the time of potential-core closing. The presence of a velocity deficit and a vorticity excess on the jet axis at that time, and the consecutive emission of sound waves are clearly visible in the resulting flow and pressure fields.

I. Introduction

After more than fifty years of research, the nature and the characteristics of the acoustic sources are well established for supersonic jets,[1] but this is not the case for subsonic jets due to limited knowledge of turbulence of jet flows.[2] For subsonic jets, the number of sources itself has been a matter of debate for a long time. Recent and past experimental[2–4] and numerical[5–7] results suggest, however, that subsonic jet noise includes two components. One is a broadband component with a relatively uniform directivity, which has been identified as the noise of the fine-scale turbulence of the jet flow.[8] Another is a low-frequency component, dominant in the downstream direction, which has been attributed to the large-scale turbulent structures of the flow.

The downstream noise component of subsonic jets appears to be produced in the vicinity of the end of the potential core, where the mixing layers merge. This contention is supported by the source distributions obtained in the jets along the axial direction using source localization techniques,[9–11] but also by cross-correlations calculated between flow quantities inside the jets and sound pressure outside.[3,7,12–18] Significant values of correlations are indeed found between flow on the jet axis near the end of the potential core and pressure radiated at small angles relative the downstream direction. Unfortunately, the corresponding noise generation mechanism is not clearly understood. It seems, however, to be related to the fact that at the end of the potential core, flow intermittency is strong, and shear-layer turbulent structures intrude quasi-periodically into the jet.[5]

*CNRS Research Scientist, AIAA Senior Member & Associate Fellow, christophe.bogey@ec-lyon.fr

In a recent work,[19] a temporally-developing subsonic round jet at a diameter-based Reynolds numbers of 3,125 was computed using direct numerical simulation, in order to investigate the noise generation mechanism mentioned above in a new and original way. Indeed, although temporal simulations have been performed in several studies for turbulent wall-bounded flows[20–22] and mixing layers,[23–25] in particular for aeroacoustic purposes in the latter case,[26–29] very few have been carried out for jets.[30] This is certainly because temporal jets do not exit from a nozzle, and have a potential core of infinite spatial length, which renders the comparisons with spatially-developing jets difficult. Despite this, for the temporal jet simulated, it was shown that when the potential core closes, mixing-layer turbulent structures intermittently intrude, accelerate and merge on the jet axis. Simultaneously, strong low-frequency acoustic waves, significantly correlated with the centerline flow fluctuations, are emitted in the downstream direction. These results are very similar to those obtained at the end of the potential core of spatially-developing subsonic jets. This suggests that the same sound source due to the potential-core closing, radiating mainly in the downstream direction, is found in temporal and spatial jets.

In the present paper, the flow and acoustic fields obtained for two temporally-developing isothermal round jets at a Mach number of 0.9 and diameter-based Reynolds numbers of 3,125 and 12,500 by solving the unsteady compressible Navier-Stokes equations using high-order finite-difference schemes are presented. The first jet is that of the previous work,[19] but ten runs, instead of five, are performed in each case in order to obtain better converged statistics. The first objective is to determine whether the observations made for the lower Reynolds number jet are also valid for the higher Reynolds number jet, *i.e.* whether the latter jet also generates low-frequency sound waves in the downstream direction in the same way as spatially-developing subsonic jets. The second objective is to find connections between these waves and the potential-core closing. With this aim in view, cross-correlations are estimated between flow quantities on the jet axis and sound pressure outside the jet flow to track causal links between sources and observer. Conditional averages of the jet near fields are also calculated in order to extract the acoustic waves resulting from the potential-core closing from the background noise. For that, the trigger condition used for the selection of samples will be related to a flow even occurring during that closing. More precisely, it will be satisfied when the minimum values of axial velocity on the jet axis due to the intermittent intrusion of turbulent structure in the jet is below an arbitrary threshold value.

The paper is organized as follows. The main characteristics of the jets and of the simulations, including initial conditions, numerical methods, grid and computational parameters, are documented in section II. The simulation results, namely vorticity and pressure snapshots, the main characteristics of the jet velocity and pressure fields, flow-noise cross-correlations, and conditional samplings of the jet near fields are shown in section III. Finally, concluding remarks are given in section IV.

II. Parameters

A. Jet definition

The two jets are round and isothermal, and are characterized by a Mach number of $\mathrm{M} = u_j/c = 0.9$ and Reynolds numbers of $\mathrm{Re}_D = u_j D/\nu = 3,125$ and $12,500$, where u_j and $D = 2r_0$ are the jet initial centerline velocity and diameter, and c and ν are the speed of sound and kinematic molecular viscosity. The ambient temperature and pressure are $T_a = 293$ K and $p_a = 10^5$ Pa. At initial time $t = 0$, the hyperbolic-tangent profiles of axial velocity presented in figure 1(a) are considered. The momentum thickness of the mixing layer is set to $\delta_\theta = 2r_0/\sqrt{\mathrm{Re}_D} = 0.0358 r_0$ for $\mathrm{Re}_D = u_j D/\nu = 3,125$ and $\delta_\theta = 0.0179 r_0$ for $\mathrm{Re}_D = 12,500$, following the variations of δ_θ/r_0 with the Reynolds number observed in experiments for initially laminar jets, e.g. in Zaman.[31] This leads to momentum Reynolds numbers of $\mathrm{Re}_\theta = u_j \delta_\theta/\nu = 56$ and 112, respectively. Radial and azimuthal velocities are set to zero, pressure is equal to p_a, and density is determined by a Crocco-Busemann relation.

At $t = 0$, velocity perturbations of low amplitude are added in the mixing layers in order to seed the laminar-turbulent transition. For this, as proposed in Bogey *et al.*,[5] divergence-free Gaussian ring vortices of radius r_0 are imposed. These vortices have a half-width of $2\delta_\theta$, and are regularly distributed in the axial direction every $\Delta z = 0.025 r_0$, where Δz is the axial mesh spacing. At each position, the vortex has a maximum velocity randomly fixed between 0 and $0.01 u_j$, and is weighted in the azimuthal direction by the function $\cos(n_\theta \theta + \varphi)$ where n_θ and φ are randomly chosen between 0 and 32 and between 0 and 2π, respectively. This allows a peak turbulence intensity of about 1% to be reached at $t = 0$. Finally, note that ten runs are performed in each case using different random seeds in order to obtain better converged

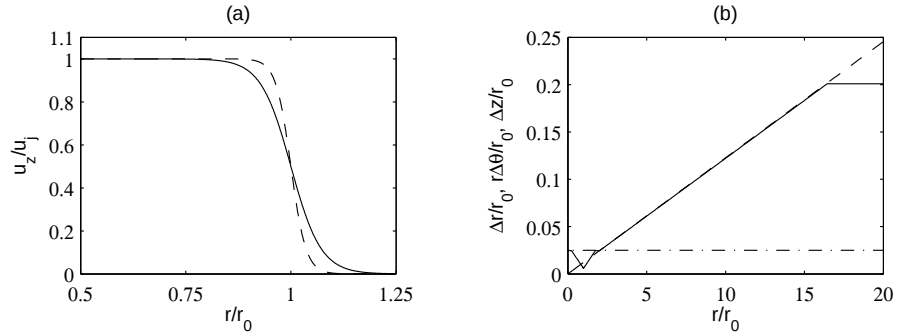

Figure 1. Radial profiles of (a) axial velocity u_z/u_j at $t = 0$ for ——— $\mathrm{Re}_D = 3,125$ and − − − $\mathrm{Re}_D = 12,500$, and (b) radial, azimuthal and axial mesh spacings ——— $\Delta r/r_0$, − − − $r\Delta\theta/r_0$ and − · − · $\Delta z/r_0$.

statistical results.

B. Numerical methods

The numerical framework is identical to that used in recent simulations of round jets.[32–35] The simulations are carried out using an in-house solver of the three-dimensional filtered compressible Navier-Stokes equations in cylindrical coordinates (r, θ, z) based on low-dissipation and low-dispersion, high-order explicit schemes. The axis singularity is taken into account by the method of Mohseni & Colonius.[36] In order to alleviate the time-step restriction near the cylindrical origin, the derivatives in the azimuthal direction around the axis are calculated at coarser resolutions than permitted by the grid.[37] For the points closest to the jet axis, they are evaluated using 16 points, yielding an effective resolution of $2\pi/16$. Fourth-order eleven-point centered finite differences are used for spatial discretization, and a second-order six-stage Runge-Kutta algorithm is implemented for time integration.[38] A twelfth-order eleven-point centered filter is applied explicitly to the flow variables every time step in order to remove grid-to-grid oscillations while leaving larger scales mostly unaffected. Non-centered finite differences and filters are also used near the grid boundaries.[32,39] The radiation conditions of Tam & Dong[40,41] are applied at the sideline boundaries to avoid significant acoustic reflections. Since a temporally-developing flow is considered, periodic boundary conditions are imposed in the axial direction.

C. Simulation parameters

The mesh grid used in the different runs extends up to $z = 120r_0$ in the axial direction, and out to $r = 30r_0$ in the radial direction. It contains $n_r \times n_\theta \times n_z = 382 \times 512 \times 4,800 = 940$ million points. The mesh spacing in the axial direction is uniform and equal to $\Delta z = 0.025r_0$, whereas, as illustrated in figure 1(b), the mesh spacing in the radial direction varies. The latter is minimum and equal to $\Delta r = 0.006r_0$ at $r = r_0$. It is maximum and equal to $\Delta r = 0.2r_0$ for $r \geq 16r_0$, yielding a Strouhal number of $\mathrm{St}_D = 2.8$ for an acoustic wave discretized by four points per wavelength. The use of $n_\theta = 512$ points in the azimuthal direction leads to $r\Delta\theta = 0.012r_0$ at $r = r_0$. Note that the simulations have been checked, from the calculation of the turbulent kinetic energy budgets, to be fully resolved direct numerical simulations for the jet at $\mathrm{Re}_D = 3,125$ and very well resolved large-eddy simulations for the jet at $\mathrm{Re}_D = 12,500$.

The computations are performed using an OpenMP-based in-house solver on 32-core nodes of Intel E5-4650 processors with a clock speed of 2.7 GHz and 16-core nodes of Intel E5-2670 processors at 2.6 GHz. The total number of iterations is equal to 22,600 for $\mathrm{Re}_D = 3,125$ and to 13,600 for $\mathrm{Re}_D = 12,500$, allowing a final time of $t = 75r_0/u_j$ to be reached. The time step Δt is chosen so that $\Delta t = 0.6\Delta r(r = r_0)/c$ for $\mathrm{Re}_D = 3,125$, and $\Delta t = \Delta r(r = r_0)/c$ for $\mathrm{Re}_D = 12,500$, ensuring the stability of the explicit time integration. For the present grid of about one billion points, 200 GB of memory are required, and about 1,000 CPU hours are consumed for 1,000 iterations. Density, the three velocity components, pressure and vorticity norm are recorded on the jet axis at $r = 0$ and on the cylindrical surfaces at $r = r_0$, $4r_0$ and $20r_0$, at a sampling frequency allowing spectra to be computed up to $\mathrm{St}_D = 10$, and on the four azimuthal planes at $\theta = 0$, $\pi/2$, π and $3\pi/2$, at half the frequency mentioned above. The statistical results obtained in each run are averaged over the periodic directions z and θ. The results of the ten runs are then ensemble

averaged, providing mean values, denoted by $< . >$ in what follows, calculated over a distance of $1,200r_0$ in the streamwise direction.

III. Results

A. Vorticity and pressure snapshots

Snapshots of the vorticity norm and pressure fluctuations obtained in the (z, r) plane for $\mathrm{Re}_D = 3,125$ at times $tu_j/r_0 = 15$, 25, 35 and 45, and for $\mathrm{Re}_D = 12,500$ at $tu_j/r_0 = 10$, 20, 30 and 40 are represented in figures 2 and 3, respectively.

For both Reynolds numbers, two mixing layers can be seen on both sides of the jet axis in the top pictures. They have just rolled up following the growth of instability waves in the hyperbolic-tangent velocity profile[42] for $\mathrm{Re}_D = 3,125$, whereas they appear to be turbulent for $\mathrm{Re}_D = 12,500$. In the second pictures from top, the mixing layers, which have developed thanks to the vortex-pairing mechanism,[43] merge on the jet axis, resulting in the disappearance of the potential core. Finally, in the third and fourth pictures, the jets are fully developed, and contain vortical scales of intensity decreasing with time. Furthermore, more fine turbulent scales are observed in the higher Reynolds number jet, as expected.

For $\mathrm{Re}_D = 3,125$, in figure 2, alternatively positive and negative fluctuations are found at $tu_j/r_0 = 15$ in the pressure field in the close vicinity of the jet. They are most likely the footprints of the coherent turbulent structures of the jet flow in the near field.[44,45] At $tu_j/r_0 = 25$, as the potential core closes, high-amplitude waves are emitted in the downstream direction. These waves are well visible at later times $tu_j/r_0 = 35$ and 45. They appear to be symmetric with respect to the jet centerline and to have a typical wavelength of about $15r_0$, Moreover, they propagate mainly in the downstream direction, and have a very large spatial extent along the wave front direction. Interestingly, they look like the waves emitted at shallow angles by spatially-developing subsonic jets.[5,6]

For $\mathrm{Re}_D = 12,500$, in figure 3, the pressure field exhibits, unsurprisingly, more high-frequency waves than for $\mathrm{Re}_D = 3,125$, but also additional noise components. Sound waves generated by potential vortex pairings in the mixing layers may for instance be noted at times $tu_j/r_0 = 10$ and 20. Upstream-propagating high-frequency waves are also clearly detected at $tu_j/r_0 = 30$ and 40, which was not the case previously. After the jet potential-core closing, however, the downstream-propagating low-frequency waves reported above for $\mathrm{Re}_D = 3,125$ are still noticeable, albeit at a lower amplitude. Therefore, they seem to persist at a higher Reynolds number.

B. Properties of the velocity fields

The mean and rms values of axial velocity calculated for the jets are represented in figure 4 using (t, r) coordinates. The results bear striking similarities with the flow fields measured in the (z, r) plane of spatially-developing subsonic jets.[46] The mean axial velocity fields of figures 4(a,b) show the jet development with time, and indicates that the potential core closes much earlier in the higher Reynolds number case, typically at $tu_j/r_0 \simeq 21$ for $\mathrm{Re}_D = 3,135$ and at $tu_j/r_0 \simeq 16$ for $\mathrm{Re}_D = 12,500$. In parallel to the mean flow development, the axial turbulence intensities are found in figure 4(c,d) to grow in the jet shear layer, to reach values slightly higher than 20%, and then to decrease. The peak values are obtained around $tu_j/r_0 = 21$ for $\mathrm{Re}_D = 3,135$ and $tu_j/r_0 = 8$ for $\mathrm{Re}_D = 12,500$, that is near the time of potential-core closing in the first case, but significantly before in the second case.

The time variations of the shear-layer momentum thickness, of the mean centerline axial velocity, and of the jet half-width are plotted in figure 5. In figure 5(a), the shear layers appear to spread slowly when the jet flows are laminar or turbulent, but more rapidly during the laminar-turbulent transitional periods, which happen between $tu_j/r_0 \simeq 12.5$ and 25 for $\mathrm{Re}_D = 3,125$, and between $tu_j/r_0 \simeq 5$ and 12.5 for $\mathrm{Re}_D = 12,500$. In figure 5(b), the velocity decay after the potential-core closing starts at $t_c u_j/r_0 = 21.6$ for $\mathrm{Re}_D = 3,125$ and $t_c u_j/r_0 = 16$ for $\mathrm{Re}_D = 3,125$, where t_c is defined by $< u_z(t_c) >= 0.95u_j$. Then, it occurs faster in the lower Reynolds number case. As for the jet half-widths in figure 5(c), they are first constant and equal to the jet initial radii, slightly decrease when the centerline velocity begins to decay, and finally increase as the jets develop. The slight decrease around $t = t_c$ may be caused by the merging of the shear layers on the jet axis when the potential core closes.

The time variations of the rms values and of the skewness and kurtosis factors of axial velocity fluctuations at $r = 0$ and $r = r_0$ are displayed in figure 6. In figure 6(a), strong humps are obtained in the profiles of

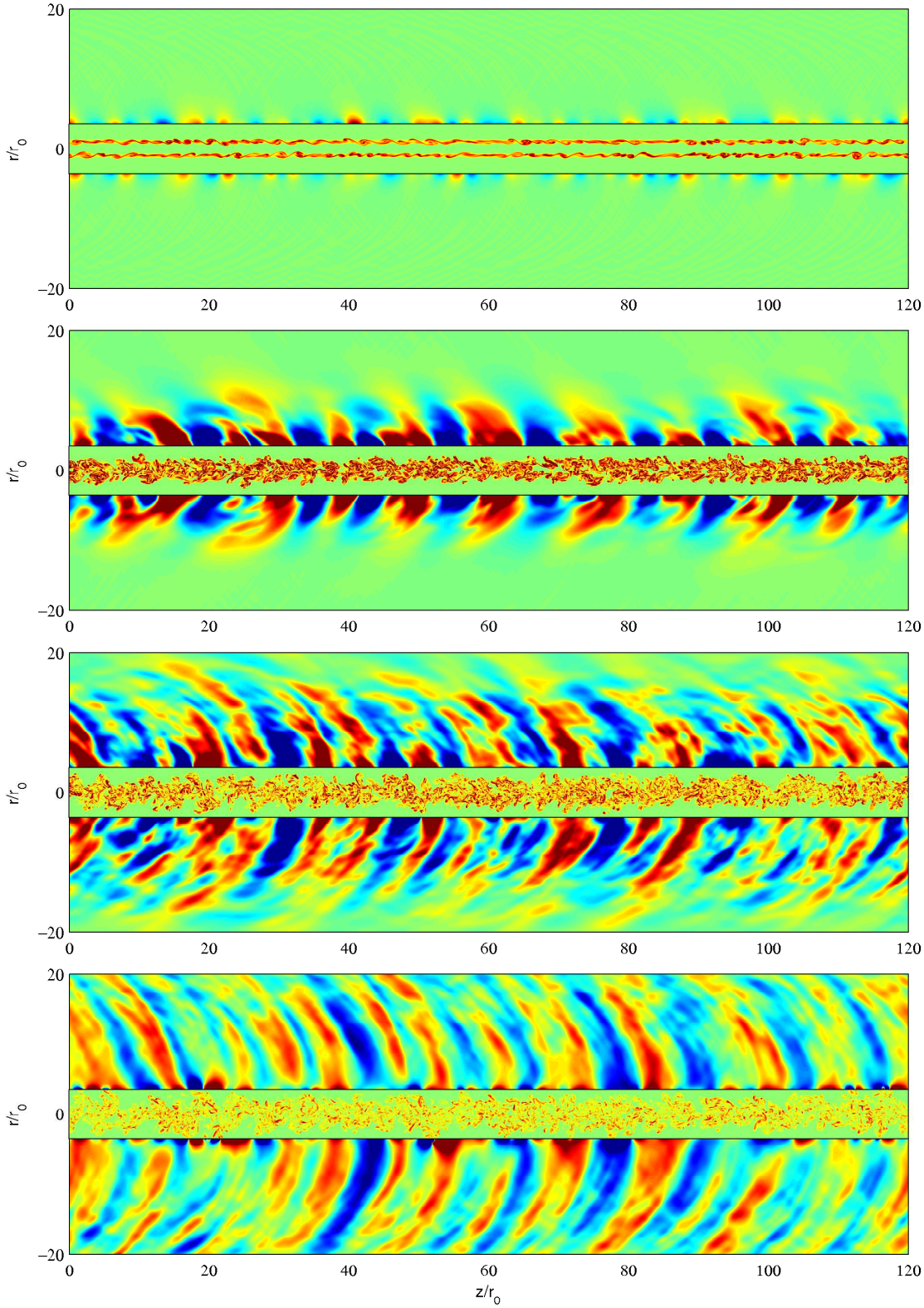

Figure 2. Representation of vorticity norm inside the jet flow and of pressure fluctuations outside, obtained for $\mathrm{Re}_D = 3,125$ at $tu_j/r_0 = 15$, 25, 35 and 45, from top to bottom. The color scales range up to the level of $4u_j/r_0$ for vorticity, and from -200 Pa to 200 Pa for pressure.

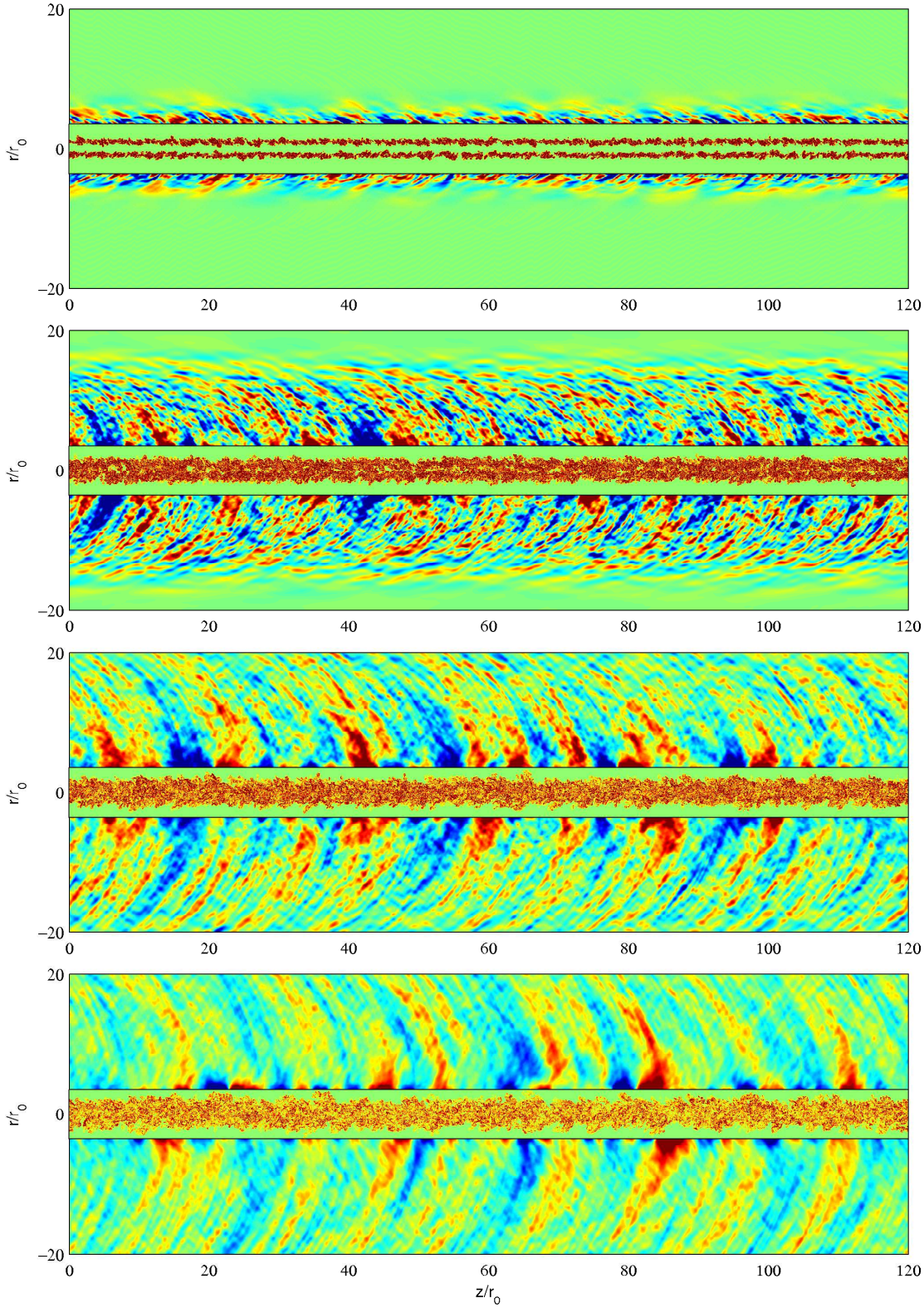

Figure 3. Representation of vorticity norm inside the jet flow and of pressure fluctuations outside, obtained for $\mathrm{Re}_D = 12,500$ at $tu_j/r_0 = 10$, 20, 30 and 40, from top to bottom. The color scales range up to the level of $4u_j/r_0$ for vorticity, and from -160 Pa to 160 Pa for pressure.

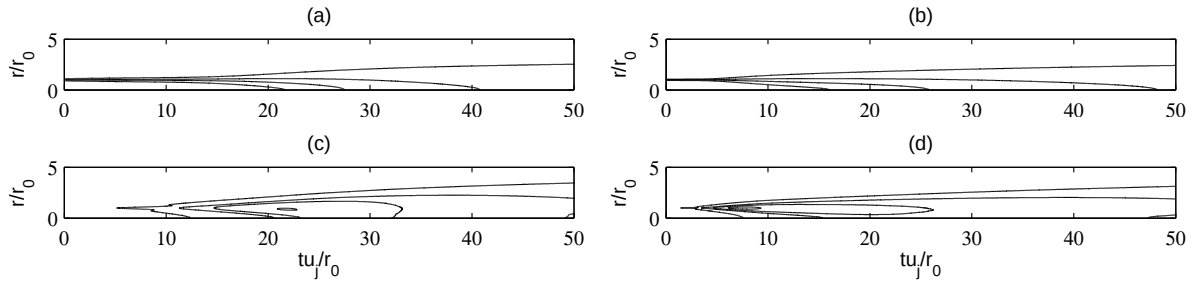

Figure 4. Space-time representation of (top) mean and (bottom) rms fields of axial velocity for (left) $\mathrm{Re}_D = 3,125$ and (right) $\mathrm{Re}_D = 12,500$ using the contour line values of: (a,b) $< u_z > / u_j = 0.05$, 0.35, 0.65 and 0.95, (c,d) $< u_z' u_z' >^{1/2} / u_j = 0.02$, 0.08, 0.14 and 0.20.

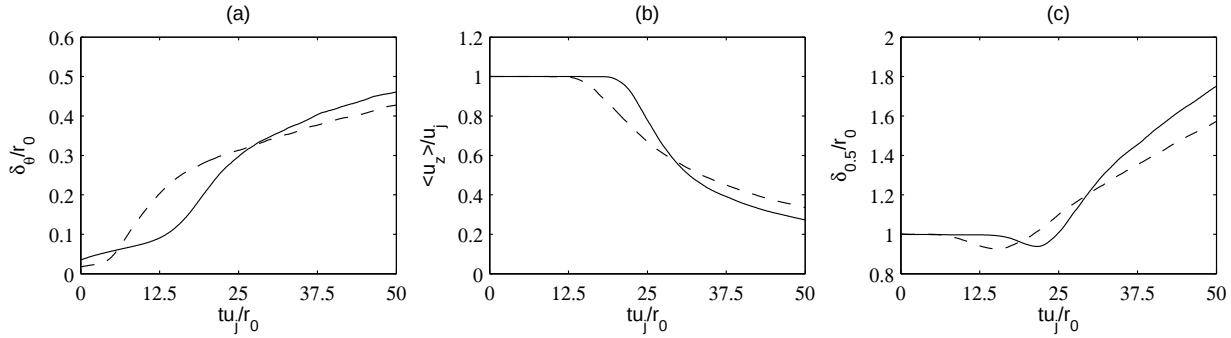

Figure 5. Time variations of (a) shear-layer momentum thickness δ_θ / r_0, (b) mean axial velocity $< u_z > / u_j$ at $r = 0$, and (c) jet half-width $\delta_{0.5} / r_0$.

turbulence intensity, leading to maximum values of 17% at $r = 0$ and 20% at $r = r_0$ for $\mathrm{Re}_D = 3,125$, and of 12.6% at $r = 0$ and 21.3% at at $r = r_0$ for $\mathrm{Re}_D = 12,500$. They result from the mergings of vortical structures[32] in the shear layers and on the jet centerline, respectively. As expected, due to the difference in mean flow development, they occur more rapidly in the $\mathrm{Re}_D = 12,500$ case. Moreover, the peak value at $r = r_0$ is reached much earlier than the peak value at $r = 0$ for $\mathrm{Re}_D = 12,500$, but that is not true for $\mathrm{Re}_D = 3,125$. This suggests the presence of vortex pairings in the mixing layers only in the high Reynolds number jet.

In figures 6(b) and 6(c), values of skewness around -1.1 and values of kurtosis higher than 6 are found at $r = 0$ close to the time of potential-core closing for both Reynolds numbers. This indicates intermittent occurrence of velocity deficits on the jet centerline at that time. They very probably follow the intrusion of shear-layer turbulent structures in the potential core of the temporal jet, as it happens at the end of the potential core of spatially-developing jets.[5,7] At $r = r_0$, the results are quite different from those at $r = 0$. In this case, the kurtosis factor does not deviate appreciably from the value of 3, but the skewness factor is slightly positive, suggesting possible bursts of high-velocity flow structures in the mixing layers.

C. Properties of the pressure fields

The rms values of pressure fluctuations obtained for the jets are represented in figure 7 using (t, r) coordinates. As previously for the velocity, the results resemble the rms pressure fields acquired in the (z, r) plane of spatially-developing subsonic jets.[46–48] For both Reynolds numbers, the maximum values are located in the jet flows, approximately at the same position as the maximum rms values of axial velocity in figure 5(c,d). Outside the jets, lobes, whose origin seems to be the peak levels in the flow, are found. They reveal the production of noise in the jet and its propagation outside with increasing time. The rms pressure fields moreover suggest that the dominant acoustic waves are generated close to the time of potential-core closing for $\mathrm{Re}_D = 3,125$, but well before for $\mathrm{Re}_D = 12,500$, and that their main radiation angle with respect to the flow direction is larger in the latter case than in the former.

The time variations of the rms values and of the skewness and kurtosis factors of the pressure fluctuations at $r = 10 r_0$ are represented in figure 8. In figure 8(a), the rms pressure profiles reach maximum values of

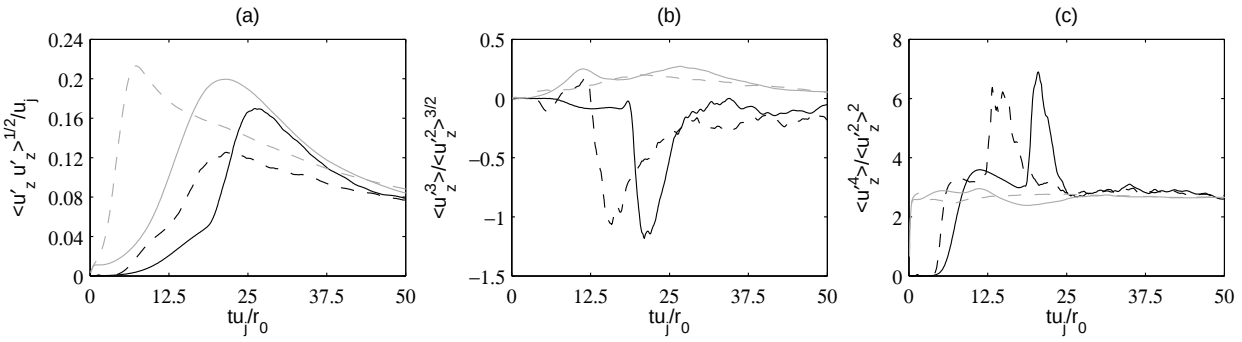

Figure 6. Time variations of (a) axial turbulence intensity $< u_z' u_z' >^{1/2} / u_j$, and (b) the skewness factor and (c) the kurtosis factor of axial velocity fluctuations u_z': at $r = 0$ for ——— $\mathrm{Re}_D = 3,125$ and − − − $\mathrm{Re}_D = 12,500$, and at $r = r_0$ for ——— $\mathrm{Re}_D = 3,125$ and − − − $\mathrm{Re}_D = 12,500$.

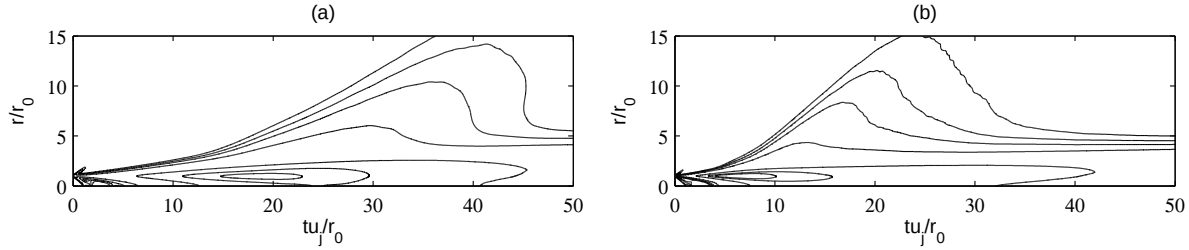

Figure 7. Space-time representation of the rms fields of pressure fluctuations for (a) $\mathrm{Re}_D = 3,125$ and (b) $\mathrm{Re}_D = 12,500$ using the contour line values of $<p'p'>^{1/2}$= 45, 60, 80, 140, 1000, 3000 and 5000 Pa.

83 Pa at $tu_j/r_0 = 35.4$ for $\mathrm{Re}_D = 3,125$ and of 68 Pa at $tu_j/r_0 = 19$ for $\mathrm{Re}_D = 12,500$. Given the times of potential-core closing, equal to $t_c u_j/r_0 = 21.6$ in the first case and to $t_c u_j/r_0 = 16$ in the second case, the peak for $\mathrm{Re}_D = 3,125$ may be due to the merging of the mixing layers on the jet axis, but it cannot true for $\mathrm{Re}_D = 12,500$. In this case, it most likely result from vortex pairings in the shear layers. As for the skewness factor in figure 8(b) and the kurtosis factor in figure 8(c), significant positive values and values different from the value of 3 are respectively obtained at the early growth stages of the acoustic levels. At later times, they are close to 0 and 3, indicating that non-linear effects and intermittency are negligible in the near fields of the present subsonic jets.

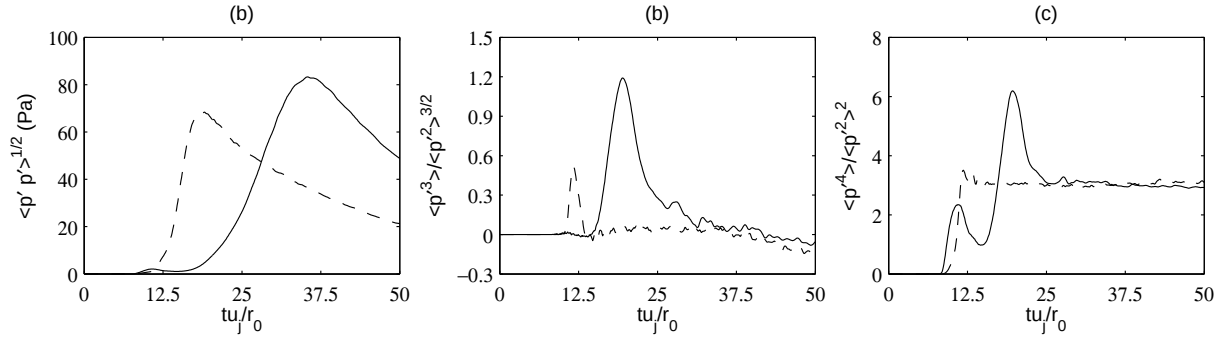

Figure 8. Time variations of (a) the rms values and (b) the skewness and (c) the kurtosis factors of the pressure fluctuations p' at $r = 10r_0$ for ——— $\mathrm{Re}_D = 3,125$ and − − − $\mathrm{Re}_D = 12,500$.

D. Flow-noise cross-correlations

In order to identify causal links between the flow and sound fields of the jets, it is interesting to compute cross-correlations between flow quantities in the jet and pressure outside, as was done in several recent experimental and numerical investigations for spatially-developing jets.[3,7,12–18] In the present work, cross-correlations between centerline flow quantities, namely axial velocity fluctuations u_z', $u_z' u_z'$ and vorticity

fluctuations $|\omega|'$, and near-field pressure fluctuations p' at $r = 10r_0$ are calculated. For u'_z, for example, they are given by

$$\mathcal{C}_{u'_z p'}(\delta z, t_1) = \frac{\langle u'_z(r_1, \theta, z + \delta z, t_1) p'(r_2, \theta, z, t_2) \rangle}{\langle u'^2_z(r_1, \theta, z + \delta z, t_1) \rangle^{1/2} \langle p'^2(r_2, \theta, z, t_2) \rangle^{1/2}}$$

The flow quantities at position $(r = r_1, z+\delta z)$ at time $t = t_1$ are thus correlated with the pressure fluctuations at position $(r = r_2, z)$ at $t = t_2$, with $r_1 = 0$ and $r_2 = 10r_0$.

The correlation maps obtained from the pressure at $t_2 u_j / r_0 = 40$ for $\mathrm{Re}_D = 3,125$ are displayed in figure 9. The dashed line represents the time of potential-core closing, and the solid line indicates a propagation at the ambient speed of sound between the centerline and the near-field points. High levels of correlations are found at the intersection of the two lines for negative separation distances δz. This supports the presence of a sound source on the jet axis, radiating in the downstream direction, when the shear layers merge. The correlations are negative for u'_z and positive for $u'_z u'_z$ and $|\omega|'$. They can be related to the intermittent arrival of low-velocity vortical structures in the jet core. Strong correlations also appear before the time of potential-core closing for vorticity, and afterward for u'_z and $u'_z u'_z$. They are very probably due to the convection of the sound sources in the jet flow. Moreover, in figure 9(a), an extra spot of positive correlations is seen at the left hand side of the spot of negative correlations, *i.e.* for a larger separation distance. This may suggest that the velocity deficit resulting from the potential-core closing correlates with an acoustic wave of positive pressure, but also with a preceding wave of negative pressure. The results reported here are very similar to those for spatially-developing jets.[7]

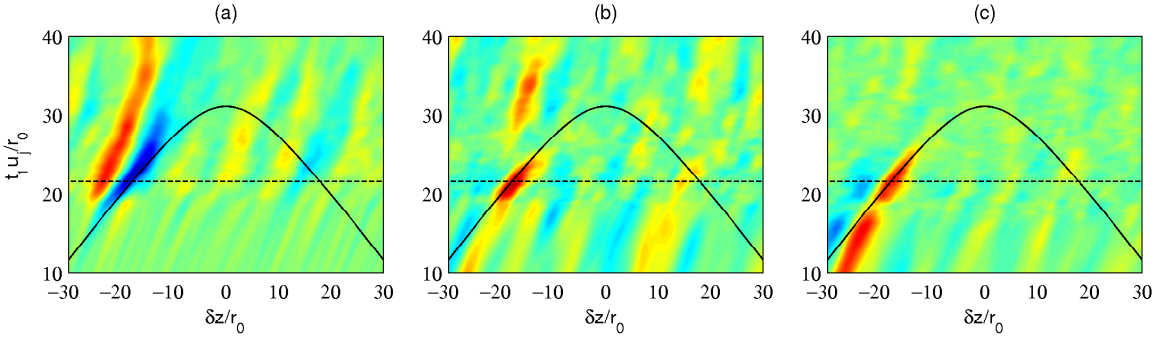

Figure 9. Space-time cross-correlations obtained for $\mathrm{Re}_D = 3,125$ between pressure fluctuations at $r = 10r_0$ and $tu_j/r_0 = 40$ and centerline flow quantities at time t_1: (a) axial velocity fluctuations u'_z, (b) the axial component of Reynolds stress tensor $u'_z u'_z$ and (c) vorticity fluctuations $|\omega|'$. The color scales range (a,c) from -0.25 to 0.25, and (b) from -0.15 to 0.15. The solid line indicates a propagation at the ambient speed of sound, and the dashed line shows the time of potential-core closing.

The correlations evaluated from the pressure at $t_2 u_j / r_0 = 35$ for $\mathrm{Re}_D = 12,500$ are presented in figure 10. Although of lower amplitude, they exhibit very similar features compared to the correlations obtained for $\mathrm{Re}_D = 3,125$. In particular, significant values of correlation are achieved at the intersection of the dashed and solid lines, as previously. Therefore, the same sound source can be expected on the centerline of the two temporal jets at different Reynolds numbers.

E. Conditional averaging of the jet flow and pressure fields

In order to better visualize the noise generation mechanism related to the intermittent intrusion of vortical structures in the core of the present jets, a conditional averaging method is applied. The method consists in averaging a limited number of samples, selected using an arbitrary trigger condition, in a signal or in a movie. It has been employed in the past in many studies to isolate a specific phenomenon from the background noise. It has thus allowed researchers, for exemple, to extract coherent structures in isotropic turbulence[49] and in mixing layers and jets,[50,51] and acoustic components in the pressure fields of free[52] and impinging[53] subsonic and supersonic jets.

In this work, the signal chosen for the sample selection is the signal of axial velocity on the jet axis at the time t_c of potential-core closing, and the trigger condition relies on the use of a threshold. The corresponding signals obtained in the first simulation runs of the two temporal jets are depicted in figure 11. For both Reynolds numbers, as expected from the profiles of skewness and kurtosis factors of velocity of

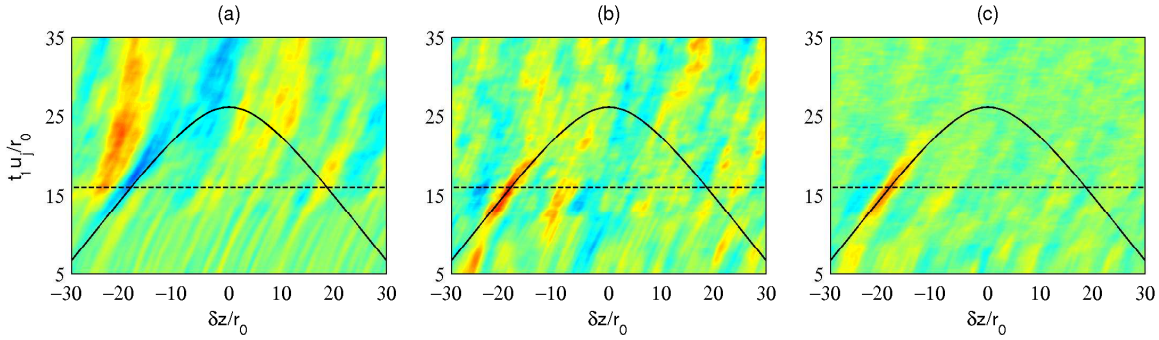

Figure 10. Space-time cross-correlations obtained for $\mathrm{Re}_D = 12,500$ between pressure fluctuations at $r = 10r_0$ and $tu_j/r_0 = 35$ and centerline flow quantities at time t_1: (a) axial velocity fluctuations u'_z, (b) the axial component of Reynolds stress tensor $u'_z u'_z$ and (c) vorticity fluctuations $|\omega|'$. The color scales range (a,c) from -0.2 to 0.2, and (b) from -0.12 to 0.12. The solid line indicates a propagation at the ambient speed of sound, and the dashed line shows the time of potential-core closing.

figure 6, intermittent negative spikes of velocity much lower than the jet velocity, even below $0.5u_j$ in certain cases, can be seen. In the conditional averaging procedure, the trigger events are identified by detecting the minimum values of velocity below $(2/3)u_j$. Those separated by a distance of less than $10r_0$ are discarded to avoid sample overlapping, reducing for instance the number of samples to 5 in the two signals of figure 11. The flow and pressure fields are then recorded over windows centered around the position z_c of the trigger events, and the resulting snapshots are ensemble averaged. This is carried out at time t_c, but also at previous and subsequent times using the same synchronization with the negative spikes of axial centerline velocity at time t_c, in order to get access to the time evolution of the noise generation mechanism. The total number of trigger events is equal to 45 for $\mathrm{Re}_D = 3,125$ and 43 for $\mathrm{Re}_D = 12,500$, and the results obtained in the four azimuthal planes at $\theta = 0$, $\pi/2$, π and $3\pi/2$ are averaged. Moreover, the use of different threshold values, namely $0.55u_j$, $0.60u_j$ and $0.75u_j$, was found not to change the results significantly.

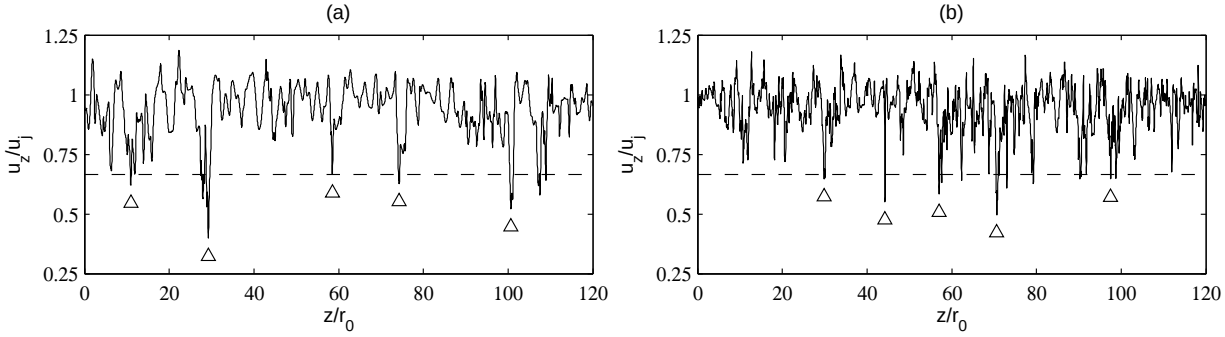

Figure 11. Representation of axial velocity u_z/u_j obtained on the jet axis for (a) $\mathrm{Re}_D = 3,125$ and (b) $\mathrm{Re}_D = 12,500$ at the time of potential core closing $t = t_c$; − − − $u_z/u_j = 2/3$; △ minimum values considered for the conditional averaging.

In what follows, given that the low-frequency downstream-propagating waves produced by the jet potential-core closing are less obvious in figure 2 for $\mathrm{Re}_D = 12,500$ than in figure 2 for $\mathrm{Re}_D = 3,125$, conditional averages are only provided for the higher-Reynolds number jet. Note however that those obtained for the lower-Reynolds number jet are very similar.

The fields of fluctuations of axial velocity, vorticity and pressure determined by conditional averaging at time t_c for the jet at $\mathrm{Re}_D = 12,500$ are represented in figure 12. Spots of strong negative and positive values, located around $z = z_c$ and of typical size r_0 in the axial direction, are observed close to the jet axis for velocity and vorticity, respectively. They indicate that the intrusion of shear-layer vortical structures in the jet when the potential core closes results in velocity deficit and vorticity excess inside the jet. Furthermore, a lobe of positive fluctuations, centered around $z = z_c$ and surrounded by two smaller lobes of negative fluctuations, is found in the pressure field. This pattern can be regarded as the footprint in the pressure field of the phenomenon of potential-core closing.

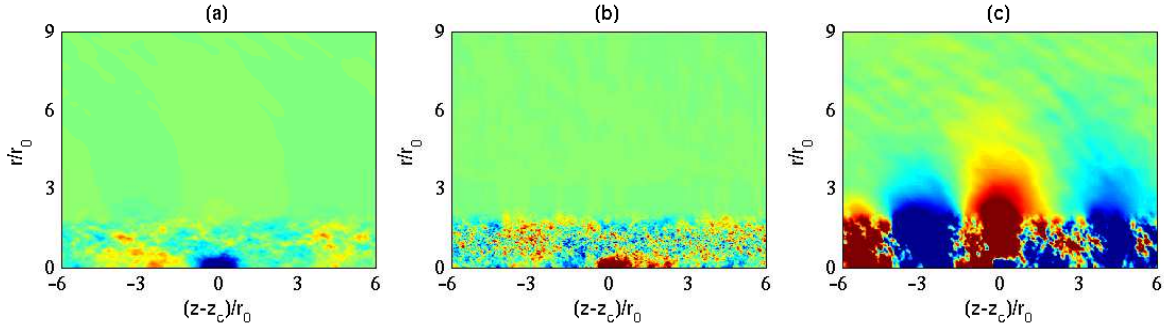

Figure 12. Representation of the fluctuations of (a) axial velocity, (b) vorticity and (c) pressure obtained for $\mathrm{Re}_D = 12,500$ at $t = t_c$ using conditional averaging. The color scales range from $-0.075u_j$ up to $0.075u_j$ for velocity, from $-0.75u_j/r_0$ up to $0.75u_j/r_0$ for vorticity, and from -200 Pa up to 200 Pa for pressure, from blue to red; z_c indicates the position of the velocity minimum values at $t = t_c$ used for the conditional averaging.

The conditional fields of pressure fluctuations obtained at three times after the potential-core closing, namely at $t = t_c + 6r_0/u_j$, $t = t_c + 12r_0/u_j$ and $t = t_c + 18r_0/u_j$, for the jet at $\mathrm{Re}_D = 12,500$ are displayed in figure 13. The aerodynamic pressure fluctuations visible at time t_c in figure 12 persist long afterward. They are centered around $z = z_c + 5r_0$ at $t = t_c + 6r_0/u_j$, $z = z_c + 8.5r_0$ at $t = t_c + 12r_0/u_j$ and $z = z_c + 11r_0$ at $t = t_c + 18r_0/u_j$. Therefore, they are convected by the jet flow at a velocity decreasing with time, due to the decay of the jet velocity for $t \geq t_c$. Outside the jet, the emission and propagation of acoustic waves in the downstream direction are clearly visible. One dominant wave of positive pressure, and two weaker waves of negative pressure on both sides, are radiated. This result provides an explanation for the multiple spots and the wavy nature of the correlations obtained between the centerline velocity and the near-field pressure in figure 10(a), but also between the centerline velocity and the downstream pressure for spatially-developing jets.[7,14]

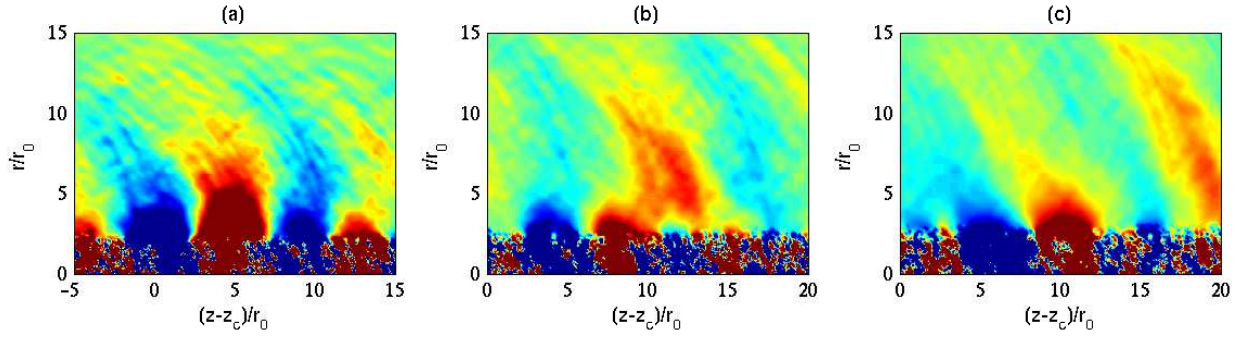

Figure 13. Representation of the pressure fluctuations obtained for $\mathrm{Re}_D = 12,500$ at (a) $t = t_c + 6r_0/u_j$, (b) $t = t_c + 12r_0/u_j$ and (c) $t = t_c + 18r_0/u_j$ using conditional averaging. The color scales range from -45 Pa up to 45 Pa, from blue to red; z_c indicates the position of the velocity minimum values at $t = t_c$ used for the conditional averaging.

IV. Conclusion

In this paper, the flow and the near pressure fields computed for temporally-developing isothermal round jets at a Mach number of 0.9 and Reynolds numbers of 3,125 and 12,500 using direct numerical simulation are presented. Cross-correlations between the two fields are also calculated in order to localize possible sound sources in the jet, and conditional averages are evaluated to extract the noise generation mechanism related to the closing of the jet potential core. Overall, despite the difference in Reynolds number, leading to a more rapid flow development and more high-frequency components for the higher-Reynolds-number jet, the results for the two jets are very similar. In both cases, when the jet mixing layers merge, high-amplitude low-frequency waves are radiated in the downstream direction. These waves are significantly correlated with

the flow fluctuations obtained on the jet centerline at the time of potential-core closing. At this time, as shear-layer turbulent structures intrude inside the jet, strong velocity deficits and vorticity excesses suddenly arise on the jet axis. As shown by the conditional sampling, performed using a synchronization with these velocity deficits, this phenomenon generates an aerodynamic pressure wavepacket in the jet and acoustic waves outside.

The results of the present work suggest that the mechanism responsible for the downstream noise component of spatially-developing subsonic jets is also encountered in temporal jets. Therefore, it does not appear to depend on the presence of a potential core of finite length, of a nozzle, or on the streamwise spreading of the jet flow. On the contrary, it seems to be intrinsically linked to the physics of the interactions between parallel mixing layers. Obviously, further studies will be required to get a better understanding of these issues.

Acknowledgments

This work was granted access to the HPC resources of FLMSN (Fédération Lyonnaise de Modélisation et Sciences Numériques), partner of EQUIPEX EQUIP@MESO, and of the resources of IDRIS (Institut du Développement et des Ressources en Informatique Scientifique) under the allocation 2016-2a0204 made by GENCI (Grand Equipement National de Calcul Intensif). It was performed within the framework of the Labex CeLyA of Université de Lyon, operated by the French National Research Agency (Grant No. ANR-10-LABX-0060/ANR-11-IDEX-0007).

References

[1]Tam, C.K.W., "Supersonic jet noise," *Annu. Rev. Fluid Mech.*, Vol. 27, 1995, pp. 17-43.

[2]Tam, C.K.W., "Jet noise: since 1952," *Theor. Comput. Fluid Dyn.*, Vol. 10, 1998, pp. 393-405.

[3]Panda, J., Seasholtz, R.G., and Elam, K.A., "Investigation of noise sources in high-speed jets via correlation measurements," *J. Fluid Mech.*, Vol. 537, 2005, pp. 349-385.

[4]Tam, C.K.W., Viswanathan, K., Ahuja, K.K., and Panda, J., "The sources of jet noise: experimental evidence," *J. Fluid Mech.*, Vol. 615, 2008, p. 253-292.

[5]Bogey, C., Bailly, C., and Juvé, D., "Noise investigation of a high subsonic, moderate Reynolds number jet using a compressible LES," *Theor. Comput. Fluid Dyn.*, Vol. 16, No. 4, 2003, pp. 273-297.

[6]Bogey, C. and Bailly, C., "Investigation of downstream and sideline subsonic jet noise using Large Eddy Simulations," *Theor. Comput. Fluid Dyn.*, Vol. 20, No. 1, 2006, pp. 23-40.

[7]Bogey, C. and Bailly, C., "An analysis of the correlations between the turbulent flow and the sound pressure field of subsonic jets," *J. Fluid Mech.*, Vol. 583, 2007, pp. 71-97.

[8]Tam, C.K.W. and Auriault, L., "Jet mixing noise from fine-scale turbulence," *AIAA J.*, Vol. 37, No. 2, 1999, pp. 145-153.

[9]Chu, W.T. and Kaplan, R.E., "Use of a spherical concave reflector for jet-noise-source distribution diagnosis," *J. Acoust. Soc. Am.*, Vol. 59, No. 6, 1976, pp. 1268-1277.

[10]Fisher, M.J., Harper-Bourne, M., and Glegg, S.A.L., "Jet engine noise source location: The polar correlation technique," *J. Sound Vib.*, Vol. 51, No. 1, 1977, pp. 23-54.

[11]Lee, S.S. and Bridges, J., "Phased-array measurements of single flow hot jets," NASA/TM 2005-213826, 2005. See also AIAA Paper 2005-2842.

[12]Lee, H.K. and Ribner, H.S., "Direct correlation of noise and flow of a jet," *J. Acoust. Soc. Am.*, Vol. 52, No. 5, 1972, pp. 1280-1290.

[13]Seiner, J.M., "The distribution of jet source strength intensity by means of direct correlation technique," Ph.D. Thesis, Pennsylvania State University, Aug. 1974.

[14]Schaffar, M., "Direct measurements of the correlation between axial in-jet velocity fluctuations and far field noise near the axis of a cold jet," *J. Sound Vib.*, Vol. 64, No. 1, 1979, pp. 73-83.

[15]Panda, J., "Experimental investigation of turbulent density fluctuations and noise generation from heated jets," *J. Fluid Mech.*, Vol. 591, 2007, pp. 73-96.

[16]Bogey, C., Barré, S., Juvé, D., and Bailly, C., "Simulation of a hot coaxial jet : direct noise prediction and flow-acoustics correlations," *Phys. Fluids*, Vol. 21, No. 3, 2009, 035105.

[17]Grizzi, S. and Camussi, R., "Wavelet analysis of near-field pressure fluctuations generated by a subsonic jet," *J. Fluid Mech.*, Vol. 698, 2012, pp. 93-124.

[18]Henning, A., Koop, L., and Schröder, A., "Causality correlation analysis on a cold jet by means of simultaneous Particle Image Velocimetry and microphone measurements," *J. Sound Vib.*, Vol. 332, 2013, pp. 3148-3162.

[19]Bogey, C., 2017, "Direct numerical simulation of a temporally-developing subsonic round jet and its sound field," AIAA Paper 2017-0925.

[20]Kim, J., Moin, P., and Moser, R., "Turbulence statistics in fully developed channel flow at low Reynolds number," *J. Fluid Mech.*, Vol. 177, 1987, pp. 133-166.

[21]Eggels, J.G.M., Unger, F., Weiss, M.H., Westerweel, J., Adrian, R.J., Friedrich, R., and Nieustadt, F.T.M., "Fully developed turbulent pipe flow: a comparison between direct numerical simulation and experiment," *J. Fluid Mech.*, Vol. 268, 1994, pp. 175-209.

[22]Kozul, M., Chung, D., and Monty, J.P., "Direct numerical simulation of the incompressible temporally developing turbulent boundary layer," *J. Fluid Mech.*, Vol. 796, 2016, pp. 437-472.

[23]Comte, P., Lesieur, M., and Lamballais, E., "Large- and small-scale stirring of vorticity and a passive scalar in a 3-D temporal mixing layer," *Phys. Fluids A*, Vol. 4, No. 12, 1992, pp. 2761-2778.

[24]Rogers, M.M. and Moser, R.D., "Direct simulation of a self-similar turbulent mixing layer," *Phys. Fluids*, Vol. 6, No. 2, 1994, pp. 903-923.

[25]Freund, J.B., Lele, S.K. and Moin, P., "Compressibility effects in a turbulent annular mixing layer. Part 1. Turbulence and growth rate," *J. Fluid Mech.*, Vol. 421, 2000, pp. 229-267.

[26]Fortuné, V., Lamballais, E., and Gervais, Y., "Noise radiated by a non-isothermal, temporal mixing layer. Part I: Direct computation and prediction using compressible DNS," *Theor. Comput. Fluid Dyn.*, Vol. 18, No. 1, 2004, pp. 61-81.

[27]Kleimann, R.R. and Freund, J.B., "The sound from mixing layers simulated with different ranges of turbulence scales," *Phys. Fluids*, Vol. 20, No. 10, 2008, 101503.

[28]Buchta, D.A., Anderson, A.T., and Freund, J.B., "Near-field shocks radiated by high-speed free-shear-flow turbulence," AIAA Paper 2014-3201, 2014.

[29]Terakado, D., Nonomura, T., Oyama, A., and Fujii, K., "Mach number dependence on sound sources in high Mach number turbulent mixing layer," AIAA Paper 2016-3015, 2016.

[30]van Reeuwijk, M. and Holzner, M., "The turbulence boundary of a temporal jet," *J. Fluid Mech.*, Vol. 739, 2014, pp. 254-275.

[31]Zaman, K.B.M.Q., "Effect of initial condition on subsonic jet noise," *AIAA J.*, Vol. 23, No. 9, 1985, pp. 1370-1373.

[32]Bogey, C. and Bailly, C., "Influence of nozzle-exit boundary-layer conditions on the flow and acoustic fields of initially laminar jets," *J. Fluid Mech.*, Vol. 663, 2010, pp. 507-539.

[33]Bogey, C., Marsden, O., and Bailly, C., "Large-Eddy Simulation of the flow and acoustic fields of a Reynolds number 10^5 subsonic jet with tripped exit boundary layers," *Phys. Fluids*, Vol. 23, No. 3, 2011, 035104.

[34]Bogey, C., Marsden, O., and Bailly, C., "Influence of initial turbulence level on the flow and sound fields of a subsonic jet at a diameter-based Reynolds number of 10^5," *J. Fluid Mech.*, Vol. 701, 2012, pp. 352-385.

[35]Bogey, C. and Marsden, O., "Simulations of initially highly disturbed jets with experiment-like exit boundary layers," *AIAA J.*, **54**(4), 2016, pp. 1299-1312.

[36]Mohseni, K. and Colonius, T., "Numerical treatment of polar coordinate singularities," *J. Comput. Phys.*, Vol. 157, No. 2, 2000, pp. 787-795.

[37]Bogey, C., de Cacqueray, N., and Bailly, C., "Finite differences for coarse azimuthal discretization and for reduction of effective resolution near origin of cylindrical flow equations," *J. Comput. Phys.*, Vol. 230, No. 4, 2011, pp. 1134-1146.

[38]Bogey, C. and Bailly, C., "A family of low dispersive and low dissipative explicit schemes for flow and noise computations," *J. Comput. Phys.*, Vol. 194, No. 1, 2004, pp. 194-214.

[39]Berland, J., Bogey, C., Marsden, O., and Bailly, C., "High-order, low dispersive and low dissipative explicit schemes for multi-scale and boundary problems," *J. Comput. Phys.*, Vol. 224, No. 2, 2007, pp. 637-662.

[40]Tam, C.K.W and Dong, Z., "Radiation and outflow boundary conditions for direct computation of acoustic and flow disturbances in a nonuniform mean flow," *J. Comput. Acoust.*, Vol. 4, No. 2,, 1996, pp. 175-201.

[41]Bogey, C. and Bailly, C., "Three-dimensional non reflective boundary conditions for acoustic simulations: far-field formulation and validation test cases," *Acta Acustica*, Vol. 88, No. 4, 2002, pp. 463-471.

[42]Michalke, A., "On the inviscid instability of the hyperbolic-tangent velocity profile," *J. Fluid Mech.*, Vol. 19, No. 4, 1964, pp. 543-556.

[43]Winant, C.D. and Browand, R.K., "Vortex pairing : the mechanism of turbulent mixing-layer growth at moderate Reynolds number," *J. Fluid Mech.*, Vol. 63, No. 2, 1974, pp. 237-255.

[44]Arndt, R.E.A, Long, D.F., and Glauser, M.N., "The proper orthogonal decomposition of pressure fluctuations surrounding a turbulent jet," *J. Fluid Mech.*, Vol. 340, 1997, pp. 1-33.

[45]Coiffet, F., Jordan, P., Delville, J., Gervais, Y., and Ricaud, F., "Coherent structures in subsonic jets: a quasi-irrotational source mechanism?," *Int. J. Aeroacoust.*, Vol. 5, No. 1, 2005, pp. 67-89.

[46]Zaman, K.B.M.Q., "Flow field and near and far sound field of a subsonic jet," *J. Sound Vib.*, Vol. 106, No. 1, 1986, p. 1-16.

[47]Ukeiley, L. and Ponton, M.K., "On the near field pressure of a transonic axisymmetric jet," *Int. J. Aeroacoust.*, Vol. 3, No. 1, 2004, pp. 43-65.

[48]Bogey, C., Barré, S., Fleury, V., Bailly, C., and Juvé, D., "Experimental study of the spectral properties of near-field and far-field jet noise," *Int. J. Aeroacoust.*, Vol. 6, No. 2, 2007, pp. 73-92.

[49]Adrian, R.J., "Conditional eddies in isotropic turbulence," *Phys. Fluids*, Vol. 22, No. 11, 1979, 2065-2070.

[50]Dahan, C., Elias, G., Maulard, J., and Perulli, M., "Coherent structures in the mixing zone of a subsonic hot free jet," *J. Sound Vib.*, Vol. 59, No. 3, 1978, pp. 313-333.

[51]Juvé, D., Sunyach, M., and Comte-Bellot, G., "Intermittency of the noise emission in subsonic cold jets," *J. Sound Vib.*, Vol. 71, No. 3, 1980, pp. 319-332.

[52]Kearney-Fisher, M., Sinha, A., and Samimy, M., "Intermittent nature of subsonic jet noise," *AIAA J.*, Vol. 51, No. 5, 2013, pp. 1142-1155.

[53]Akamine, M., Okamoto, K., Teramoto, S., Okunuki, T., and Tsutsumi, S., "Conditional sampling analysis of acoustic phenomena from a supersonic jet impinging on a inclined flat plate," *Trans. Japan Soc. Aero. Space Sci.*, Vol. 59, No. 5, 2016, pp. 287-294.